

Supplementary Materials for
**Organocatalyzed atroposelective dynamic kinetic resolutions via transient
seven-membered cyclic hemiacetals**

Qinglong Zhou *et al.*

Corresponding author: Xing Yang, xingyang@hunnu.edu.cn; Xinglong Zhang, xinglong.zhang@cuhk.edu.hk;
Yonggui Robin Chi, robinchi@ntu.edu.sg

Sci. Adv. **11**, eadx8255 (2025)
DOI: 10.1126/sciadv.adx8255

This PDF file includes:

Sections S1 to S7

Tables S1 to S4

Figs. S1 to S7

References

combined organic layer was dried over anhydrous Na₂SO₄, evaporated under reduced pressure. Then, the mixture was purified by column chromatography using silica gel (PE/EA = 10:1) to afford the crude products (including hemiacetals) **1f**, **1i**, **1k**, **1n**, **1o**.

Section S4. Mechanism studies

Computational methods for mechanism studies

Geometry optimizations in the gas phase were initially carried out using global hybrid functional M06-2X (78) with Karlsruhe-family basis set of double- ζ valence def2-SVP (85, 86) for all atoms as implemented in *Gaussian 16* rev. A.03. (87) Minima and transition structures on the potential energy surface (PES) were confirmed as such by harmonic frequency analysis, showing respectively zero and one imaginary frequency, at the same level of theory.

Single point (SP) corrections were performed using M06-2X functional and def2-TZVP (85) basis set for all atoms. The implicit SMD continuum solvation model was used to account for the solvent effects of dichloroethane (DCE) on the overall free energy PES. Gibbs energies were evaluated at the room temperature, as was used in the experiments, using a quasi-RRHO treatment of vibrational entropies. (88, 89) Vibrational entropies of frequencies below 100 cm⁻¹ were obtained according to a free rotor description, using a smooth damping function to interpolate between the two limiting descriptions. The free energies were further corrected using standard concentration of 1 mol/L, which was used in solvation calculations. SMD(DCE)-M06-2X/def2-TZVP//M06-2X/def2-SVP Gibbs energies are given and quoted in kcal mol⁻¹ throughout. *Unless otherwise stated, these solvent-corrected values are used for discussion throughout the main text and in this supporting information.*

Non-covalent interactions (NCIs) were analyzed using NCIPILOT calculations. The .wfn files for NCIPILOT were generated at M06-2X/def2-SVP (85, 86) level of theory. NCI indices calculated with NCIPILOT were visualized at a gradient isosurface value of $s = 0.5$ au. These are colored according to the sign of the second eigenvalue (λ_2) of the Laplacian of the density ($\nabla^2\rho$) over the range of -0.1 (blue = attractive) to +0.1 (red = repulsive). All molecular structures and molecular orbitals were visualized using *PyMOL* software. (90)

Model reaction

For this study, we select the model reaction depicted in Figure S1 for mechanistic studies using DFT modeling.

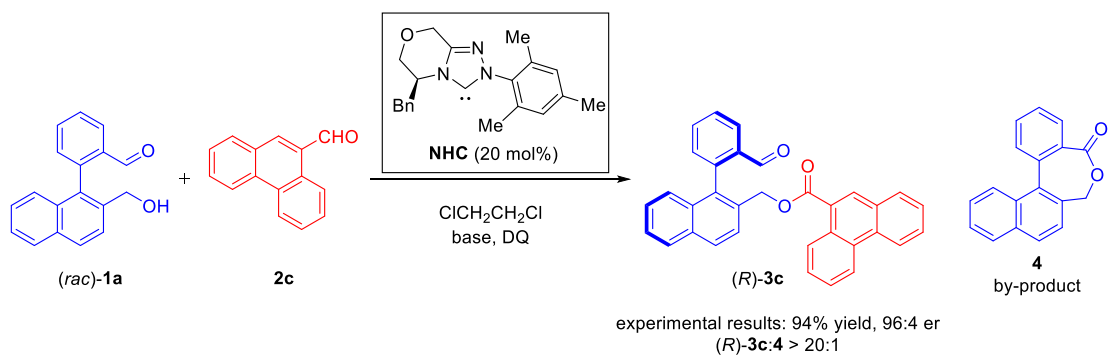


Figure S1. Model reaction used for DFT based mechanistic studies.

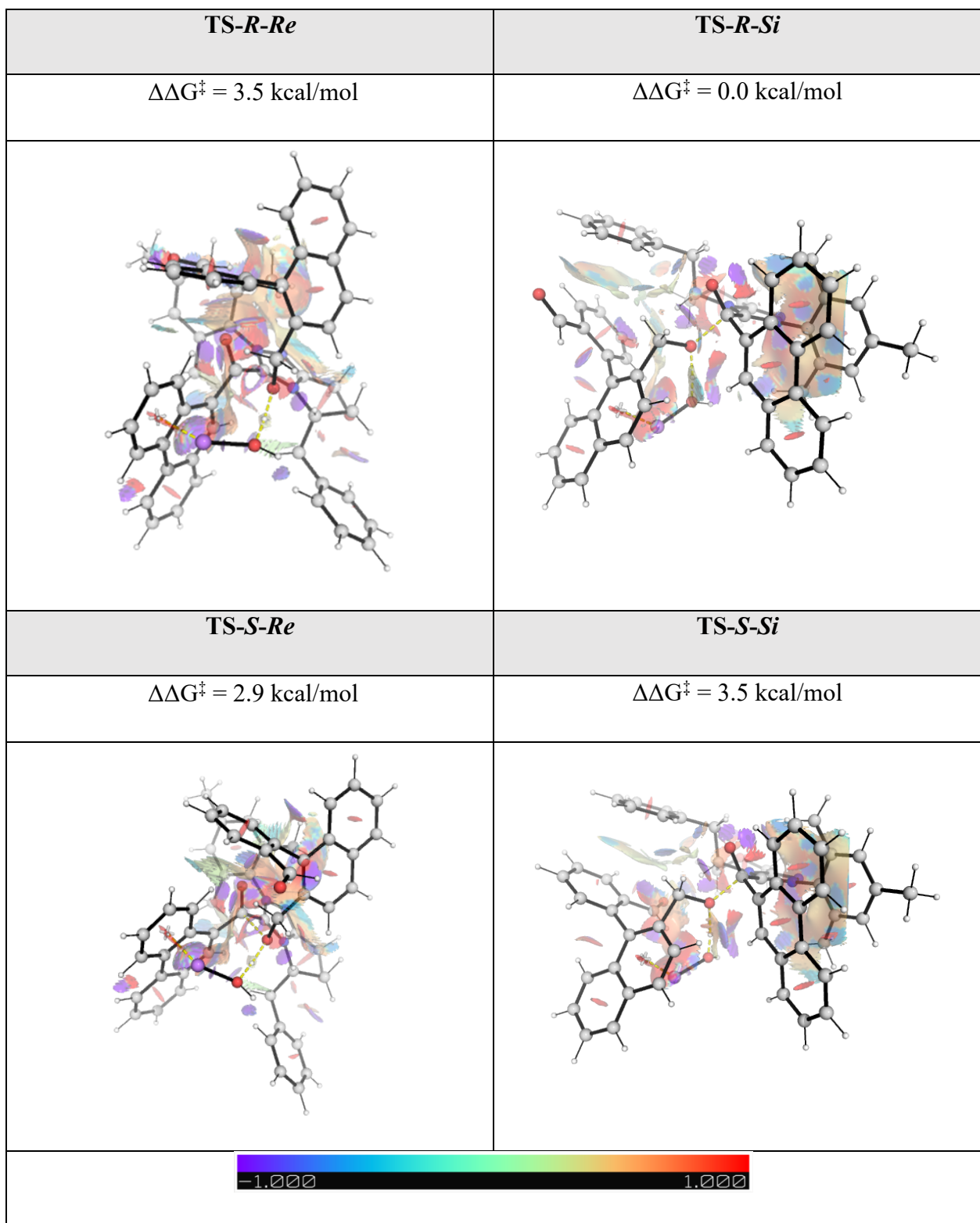


Figure S2. NCI plots for the enantio-determining TSs for the NHC catalyzed model reaction.

Distortion-interaction analysis for enantio-determining TSs

Distortion-interaction analysis is applied to enantio-determining TSs (**TS-R-Si** and **TS-S-Re**) to discern the factors affecting enantioselectivity. The transition state structures are decomposed by dividing the cationic acyl azolium intermediate **II** (formed from NHC and **2c**), and substrate **1a** with LiOH as components. Single point calculations with SMD(DCE) solvent correction were applied performed at M06-2X/def2-TZVP level of theory to obtain distortion and interaction energies. The distortion energy is given by:

$$E_{dist} = E_{TS,frag1} + E_{TS,frag2} - (E_{eq,frag1} + E_{eq,frag2})$$

where *TS,frag1,2* represent individual fragments in their distorted transition state geometries; and *eq,frag1,2* represent individual fragments in their optimized, equilibrium ground-state geometries; the interaction energy is given by:

$$E_{int} = E_{TS} - (E_{TS,frag1} + E_{TS,frag2})$$

which accounts for the stabilizing interactions (e.g., electrostatic, orbital, dispersion) between the distorted fragments in the TS.

Thus, the total activation energy is given by:

$$\Delta E^\ddagger = E_{dist} + E_{int}$$

Note that this single point activation energy and the activation energy differences $\Delta\Delta E^\ddagger$ between the TSs (**TS-R-Si** vs. **TS-S-Re**) may be different from the Gibbs energy differences $\Delta\Delta G^\ddagger$ that is computed fully (including vibrational frequencies analysis) at SMD(DCE)-M06-2X/def2-TZVP//M06-2X/def2-SVP level of theory.

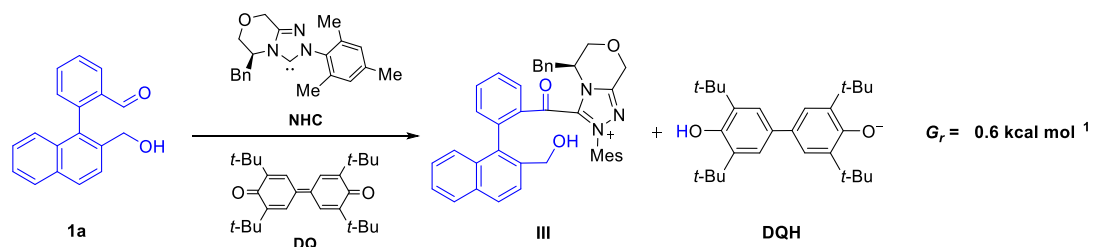
The analysis gives a $\Delta\Delta E^\ddagger$ (TS) of 3.4 kcal/mol in favor of **TS-R-Si** over **TS-S-Re**. Although **TS-R-Si** exhibits a lower stabilizing interaction energy over **TS-S-Re** ($E_{int} = -112.6$ vs. -127.3 kcal/mol), this is outweighed by its significantly lower distortion energy ($E_{dist} = 83.2$ vs. 101.3 kcal/mol), Table S4. As a result, the overall ΔE^\ddagger for **TS-R-Si** is 3.4 kcal/mol lower than that of **TS-S-Re** (-29.4 vs. -26.0 kcal/mol), rendering **TS-R-Si** the more favorable transition state, Table S4.

Table S4: Distortion-interaction analysis.

Transition State	ΔE^\ddagger	E_{dist}	E_{int}
TS- <i>R-Si</i>	-29.4	83.2	-112.6
TS- <i>S-Re</i>	-26.0	101.3	-127.3

Model reactions for the formation of acyl azonium intermediates II and III

a)



b)

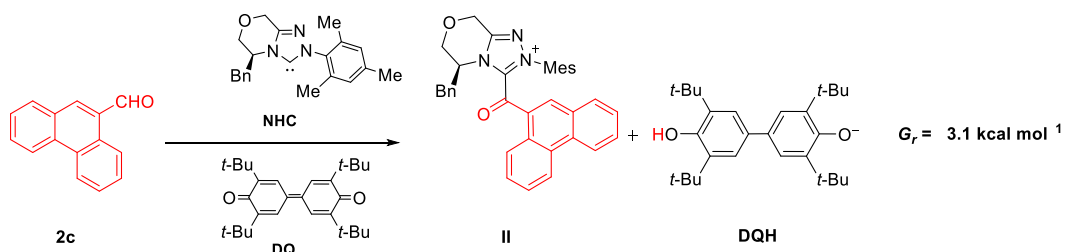


Figure S3. Model reactions employed for DFT based estimation of the reaction free energies for the formation of a) III, and b) II.

Interconversion of *R* and *S* forms of **1a'** and **4**

To estimate the free energy barrier for the interconversion of *R* and *S* forms of intermediate **1a'**, we employed two diastereomeric conformers differing at the chiral carbon center as starting geometries for dihedral rotation around the C–C bond in **1a'**, which led to the identification of transition states **TS-rot-1** and **TS-rot-2** (Figure S4a). The calculated barrier for **TS-rot-1** is 19.9 kcal/mol, which is 2.7 kcal/mol lower than that of **TS-rot-2** (22.6 kcal/mol). Similarly, the computed free energy barrier for the interconversion of *R* and *S* forms of compound **4**, via **TS-rot-4** (Figure S4b), is 22.2 kcal/mol, in excellent agreement with the experimentally determined value of 21.9 kcal/mol. This consistency supports the reliability of our computed rotational barrier for intermediate **1a'**, which could not be measured

experimentally, and suggests that it falls in a similar range of value (~20 kcal/mol).

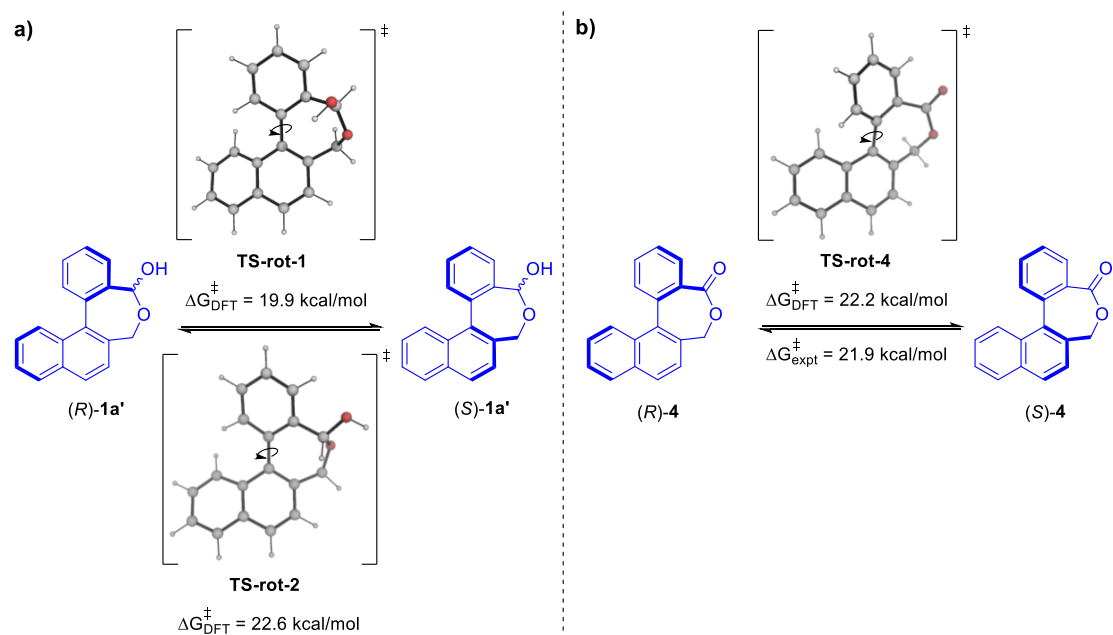


Figure S4. Interconversion of *R* and *S* forms of a) intermediate **1a'** and b) compound **4** via rotational transition state over the C–C axial axis.

Interconversion of *R* and *S* forms of substrate **1a**

We studied the rotational barriers for the enantiomerization of substrate **1a**. Initially, we carried out a relaxed PES scan of a dihedral angle along the axial C–C bond using M06-2X/def2-SVP level of theory in the gas phase (Figure S5). Our results indicate that the highest energy structures for enantiomerization (structures 2 and 5, Figure S5) are lying at ~36 kcal/mol and ~56 kcal/mol, respectively. Subsequently, using these highest energy structures as initial guess structures for TS search, we successfully located the *true* TS structures for enantiomerization via rotation along the axial C–C bond. The computed barriers are 34.8 kcal mol for **TS-rot-1a** (Figure S6), which is the rotational barrier for the aldehyde group to cross over the naphthalene side group, and 36.0 kcal/mol for **TS-rot-1b** (Figure S6), which is the rotational barrier for the aldehyde group to cross over the benzyl alcohol group. Both rotational TSs have very high barriers, indicating that direct enantiomerization of **1a** is unlikely under ambient reaction conditions. However, a lower energy pathway involving the conversion of **1a** firstly to lactol intermediate **1a'** (Figure S4a) and then its rotation about the axial C–C bond of **1a'** may enable the overall enantiomerization of **1a** via the intermediary of **1a'**.

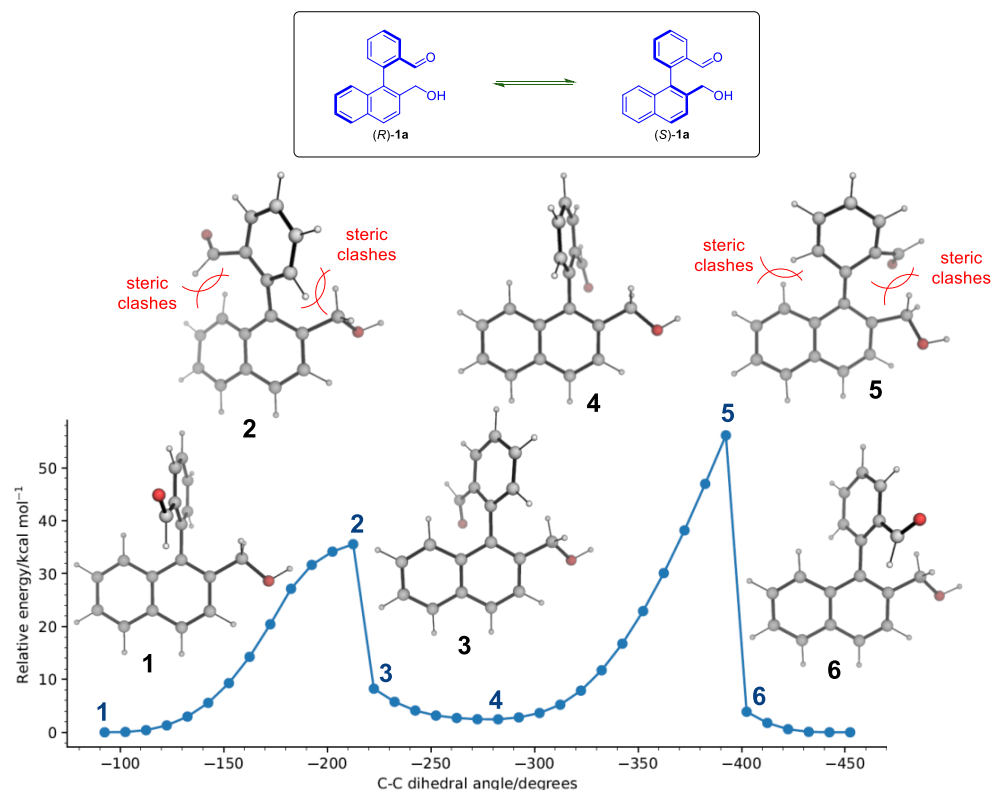


Figure S5. Relaxed potential energy surface (PES) scan for the dihedral angle along the C–C axial bond of the substrate **1a**, computed at M06-2X/def2-SVP level of theory.

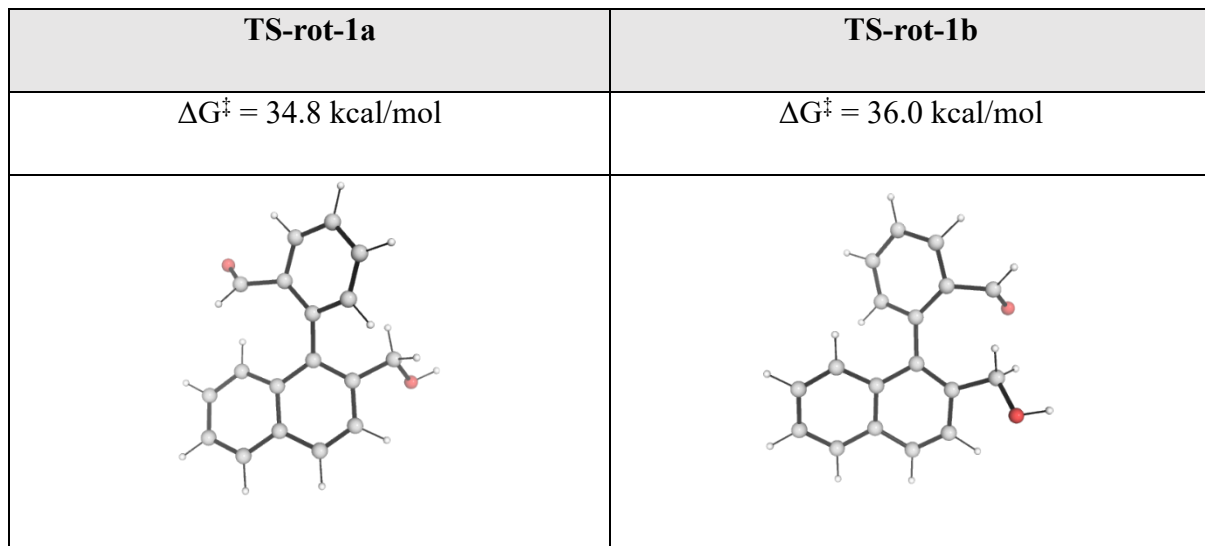


Figure S6. DFT-optimized rotational TS structures for the enantiomerization of substrate **1a**, TS-rot-1a and TS-rot-1b. Rotational barriers are calculated at SMD(DCE)-M06-2X/def2-TZVP//M06-2X/def2-SVP level of theory at room temperature and are given in kcal mol^{-1} .

Optimized structures and raw energies

Geometries of all optimized structures (in .xyz format with their associated energy in Hartrees) are included in a separate folder named *DFT_optimized_structures*. All these data have been deposited and uploaded to <https://zenodo.org/records/15774233> (DOI: 10.5281/zenodo.15774233).

Absolute values (in Hartrees) for SCF energy, zero-point vibrational energy (ZPE), enthalpy and quasi-harmonic Gibbs free energy (at 298.15K) for gas-phase M06-2X/def2-SVP optimized structures are given below. Single point corrections in SMD dichloroethane using M06-2X/def2-TZVP functional are also included.

Structure	E/au	ZPE/au	H/au	T.S/au	qh-G/au	SP MN15/def2- TZVP
NHC	-1052.302228	0.405003	-1051.874	0.075513	-1051.94366	-1053.501437
1a	-843.825362	0.273106	-843.534948	0.059848	-843.591925	-844.783629
2c	-652.108964	0.20644	-651.89008	0.047376	-651.936711	-652.8426641
R-3a	-1494.78425	0.460964	-1494.294624	0.087758	-1494.375325	-1496.459919
4	-842.656882	0.2542	-842.387955	0.05225	-842.439156	-843.6087804
DQ	-1240.022914	0.620195	-1239.369317	0.091886	-1239.456033	-1241.422698
DQH⁻	-1240.720581	0.629463	-1240.057724	0.090543	-1240.143811	-1242.179491
LiOH	-83.270079	0.012644	-83.253346	0.014279	-83.267625	-83.40038398
II	-1703.66235	0.604815	-1703.023396	0.096538	-1703.113329	-1705.620376
III	-1895.390031	0.673552	-1894.677632	0.105227	-1894.775689	-1897.561404
TS-R-Re	-2630.855321	0.893829	-2629.907483	0.138275	-2630.034388	-2633.846465
TS-R-Si	-2630.860919	0.894017	-2629.912509	0.139815	-2630.040674	-2633.851275
TS-S-Re	-2630.850654	0.893342	-2629.902844	0.141124	-2630.031256	-2633.845822
TS-S-Si	-2630.862383	0.895464	-2629.912954	0.137461	-2630.03982	-2633.847948
R-1a'	-843.840012	0.277324	-843.547328	0.053242	-843.599581	-844.7929473
TS-rot-1	-843.800491	0.277187	-843.505079	0.06163	-843.565415	-844.7558681
TS-rot-2	-843.802331	0.27673	-843.510774	0.052133	-843.561952	-844.7569107
TS-rot-1a	-843.768686	0.273675	-843.479129	0.054341	-843.532574	-844.7309058
TS-rot-1b	-843.767694	0.273508	-843.478442	0.053767	-843.531481	-844.7290457
TS-1a	-1896.145788	0.681982	-1895.42506	0.104971	-1895.52298	-1898.276139
TS-2c	-1704.425354	0.613712	-1703.77692	0.098736	-1703.86817	-1706.339554
TS-rot-4	-842.623597	0.253801	-842.35582	0.050299	-842.405519	-843.573727

REFERENCES AND NOTES

1. G. Bringmann, A. J. Price Mortimer, P. A. Keller, M. J. Gresser, J. Garner, M. Breuning, Atroposelective synthesis of axially chiral niaryl compounds. *Angew. Chem. Int. Ed.* **44**, 5384–5427 (2005).
2. E. Kumarasamy, R. Raghunathan, M. P. Sibi, J. Sivaguru, Nonbiaryl and heterobiaryl atropisomers: Molecular templates with promise for atropselective chemical transformations. *Chem. Rev.* **115**, 11239–11300 (2015).
3. Y.-B. Wang, B. Tan, Construction of axially chiral compounds via asymmetric organocatalysis. *Acc. Chem. Res.* **51**, 534–547 (2018).
4. J. A. Carmona, C. Rodríguez-Franco, R. Fernández, V. Hornillos, J. M. Lassaletta, Atroposelective transformation of axially chiral (hetero)biaryls. From desymmetrization to modern resolution strategies. *Chem. Soc. Rev.* **50**, 2968–2983 (2021).
5. C.-X. Liu, W.-W. Zhang, S.-Y. Yin, Q. Gu, S.-L. You, Synthesis of atropisomers by transition-metal–catalyzed asymmetric C–H functionalization reactions. *J. Am. Chem. Soc.* **143**, 14025–14040 (2021).
6. G. Bringmann, T. Gulder, T. A. M. Gulder, M. Breuning, Atroposelective total synthesis of axially chiral biaryl natural products. *Chem. Rev.* **111**, 563–639 (2011).
7. J. Wencel-Delord, A. Panossian, F. R. Leroux, F. Colobert, Recent advances and new concepts for the synthesis of axially stereoenriched biaryls. *Chem. Soc. Rev.* **44**, 3418–3430 (2015).
8. J. K. Cheng, S.-H. Xiang, S. Li, L. Ye, B. Tan, Recent advances in catalytic asymmetric construction of atropisomers. *Chem. Rev.* **121**, 4805–4902 (2021).
9. H.-H. Zhang, F. Shi, Organocatalytic atroposelective synthesis of indole derivatives bearing axial chirality: Strategies and applications. *Acc. Chem. Res.* **55**, 2562–2580 (2022).

10. C. B. Roos, C.-H. Chiang, L. A. M. Murray, D. Yang, L. Schulert, A. R. H. Narayan, Stereodynamic strategies to induce and enrich chirality of atropisomers at a late stage. *Chem. Rev.* **123**, 10641–10727 (2023).
11. S.-H. Xiang, W.-Y. Ding, Y.-B. Wang, B. Tan, Catalytic atroposelective synthesis. *Nat. Catal.* **7**, 483–498 (2024).
12. X. Zhang, K. Zhao, Z. Gu, Transition metal-catalyzed biaryl atropisomer synthesis via a torsional strain promoted ring-opening reaction. *Acc. Chem. Res.* **55**, 1620–1633 (2022).
13. J. Q. Shi, F. Fang, D.-J. Cheng, Organocatalytic atroposelective dynamic kinetic resolution involving ring manipulations. *Adv. Synth. Catal.* **366**, 1269–1284 (2024).
14. J. A. Carmona, C. Rodríguez-Franco, R. Fernández, J. M. Lassaletta, V. Hornillos, Lewis acid-base interactions as a racemization strategy for the atroposelective synthesis of (hetero) biaryls via dynamic kinetic resolution. *ChemCatChem* **16**, e202400701 (2024).
15. C. Wu, Y. Jin, X. Zhang, R. Gao, X. Dou, Development of configurationally labile biaryl reagents for atropisomer synthesis. *Eur. J. Org. Chem.* **27**, e202400402 (2024).
16. S. E. Huth, E. A. Stone, S. Crotti, S. J. Miller, On the ability of the N–O bond to support a stable stereogenic axis: Peptide-catalyzed atroposelective N-oxidation. *J. Org. Chem.* **88**, 12857–12862 (2023).
17. K. Zhao, L. Duan, S. Xu, J. Jiang, Y. Fu, Z. Gu, Enhanced reactivity by torsional strain of cyclic diaryliodonium in Cu-catalyzed enantioselective ring-opening reaction. *Chem* **4**, 599–612 (2018).
18. S. Yang, T. Zheng, L. Duan, X. Xue, Z. Gu, Atroposelective three-component coupling of cyclic diaryliodoniums and sodium cyanate enabled by the dual-role of phenol. *Angew. Chem. Int. Ed. Engl.* **62**, e202302749 (2023).
19. J. Han, B. Xiao, T.-Y. Sun, M. Wang, L. Jin, W. Yu, Y. Wang, D.-M. Fang, Y. Zhou, X.-F. Wu, Y.-D. Wu, J. Liao, Enantioselective double carbonylation enabled by high-valent palladium catalysis. *J. Am. Chem. Soc.* **144**, 21800–21807 (2022).

20. J. Zhang, T. Sun, Z. Zhang, H. Cao, Z. Bai, Z.-C. Cao, Nickel-catalyzed enantioselective arylative activation of aromatic C–O bond. *J. Am. Chem. Soc.* **143**, 18380–18387 (2021).
21. L. Pang, Q. Sun, Z. Huang, G. Li, J. Liu, J. Guo, C. Yao, J. Yu, Q. Li, Palladium-catalyzed stereoselective cleavage of C–P bond: Enantioselective construction of atropisomers containing a P-stereogenic center. *Angew. Chem. Int. Ed. Engl.* **61**, e202211710 (2022).
22. M. Wu, Y.-W. Chen, Q. Lu, Y.-B. Wang, J. K. Cheng, P. Yu, B. Tan, Organocatalytic Si–C aryl bond functionalization-enabled atroposelective synthesis of axially chiral biaryl siloxanes. *J. Am. Chem. Soc.* **145**, 20646–20654 (2023).
23. Y. Liu, Y.-L. S. Tse, F. Y. Kwong, Y.-Y. Yeung, Accessing axially chiral biaryls via organocatalytic enantioselective dynamic-kinetic resolution-semipinacol rearrangement. *ACS Catal.* **7**, 4435–4440 (2017).
24. Z. Zhang, J. Zhang, Q. Gao, Y. Zhou, M. Yang, H. Cao, T. Sun, G. Luo, Z.-C. Cao, Enantioselective alkylative cross-coupling of unactivated eromatic C–O electrophiles. *Nat. Commun.* **13**, 2953 (2022).
25. G. Bringmann, T. Hartung, First atropo-enantioselective ring opening of achiral biaryls containing lactone bridges with chiral hydride-transfer reagents derived from borane. *Angew. Chem. Int. Ed. Engl.* **31**, 761–762 (1992).
26. G.-Q. Chen, B.-J. Lin, J.-M. Huang, L.-Y. Zhao, Q.-S. Chen, S.-P. Jia, Q. Yin, X. Zhang, Design and synthesis of chiral oxa-spirocyclic ligands for Ir-catalyzed direct asymmetric reduction of Bringmann’s lactones with molecular H₂. *J. Am. Chem. Soc.* **140**, 8064–8068 (2018).
27. C. Yu, H. Huang, X. Li, Y. Zhang, W. Wang, Dynamic kinetic resolution of biaryl lactones via a chiral bifunctional amine thiourea-catalyzed highly atropo-enantioselective transesterification. *J. Am. Chem. Soc.* **138**, 6956–6959 (2016).

28. O. M. Beleh, E. Miller, F. D. Toste, S. J. Miller, Catalytic dynamic kinetic resolutions in tandem to construct two-axis terphenyl atropisomers. *J. Am. Chem. Soc.* **142**, 16461–16470 (2020).
29. Z. H. Luo, W. T. Wang, T. Y. Tang, S. Zhang, F. Huang, D. Hu, L. F. Tao, L. Qian, J. Y. Liao, Torsional strain-independent catalytic enantioselective synthesis of biaryl atropisomers. *Angew. Chem. Int. Ed. Engl.* **61**, e202211303 (2022).
30. G. Wang, Q. Shi, W. Hu, T. Chen, Y. Guo, Z. Hu, M. Gong, J. Guo, D. Wei, Z. Fu, W. Huang, Organocatalytic asymmetric *N*-sulfonyl amide C–N bond activation to access axially chiral biaryl amino acids. *Nat. Commun.* **11**, 946 (2020).
31. Y. Cai, Y. Zhao, K. Tang, H. Zhang, X. Mo, J. Chen, Y. Huang, Amide C–N bonds activation by A new variant of bifunctional N-heterocyclic carbene. *Nat. Commun.* **15**, 496 (2024).
32. Y. Yang, C. Wu, J. Xing, X. Dou, Developing biarylhemiboronic esters for biaryl atropisomer synthesis via dynamic kinetic atroposelective Suzuki–Miyaura cross-coupling. *J. Am. Chem. Soc.* **146**, 6283–6293 (2024).
33. L. Wei, J. Li, Y. Zhao, Q. Zhou, Z. Wei, Y. Chen, X. Zhang, X. Yang, Chiral phosphoric acid catalyzed asymmetric hydrolysis of biaryl oxazepines for the synthesis of axially chiral biaryl amino phenol derivatives. *Angew. Chem. Int. Ed. Engl.* **62**, e202306864 (2023).
34. V. Hornillos, J. A. Carmona, A. Ros, J. Iglesias-Sigüenza, J. López-Serrano, R. Fernández, J. M. Lassaletta, Dynamic kinetic resolution of heterobiaryl ketones by zinc-catalyzed asymmetric hydrosilylation. *Angew. Chem. Int. Ed. Engl.* **57**, 3777–3781 (2018).
35. Y.-D. Shao, J.-S. Feng, D.-D. Han, K.-H. Pan, L. Zhang, Y.-F. Wang, Z.-H. Ma, P.-R. Wang, M. Yin, D.-J. Cheng, Construction of axially chiral styrene-type allylamines via chiral phosphoric acid-catalyzed asymmetric reductive amination. *Org. Chem. Front.* **9**, 764–770 (2022).
36. H. X. Jiang, D. D. Han, R. P. Song, Q. Shi, X. F. He, W. Q. Kou, Q. Zhao, Y. D. Shao, D. J. Cheng, Chiral boro-phosphate catalyzed asymmetric transfer hydrogenation of 1-enal

- substituted 2-naphthols: Access to axially chiral styrene-type allylalcohols. *Adv. Synth. Catal.* **365**, 1398–1404 (2023).
37. F. Guo, S. Fang, J. He, Z. Su, T. Wang, Enantioselective organocatalytic synthesis of axially chiral aldehyde-containing styrenes via SNAr reaction-guided dynamic kinetic resolution. *Nat. Commun.* **14**, 5050 (2023).
38. K. Mori, T. Itakura, T. Akiyama, Enantiodivergent atroposelective synthesis of chiral biaryls by asymmetric transfer hydrogenation: Chiral phosphoric acid catalyzed dynamic kinetic resolution. *Angew. Chem. Int. Ed. Engl.* **55**, 11642–11646 (2016).
39. J. Zhang, J. Wang, Atropoenantioselective redox-neutral amination of biaryl compounds through borrowing hydrogen and dynamic kinetic resolution. *Angew. Chem. Int. Ed. Engl.* **57**, 465–469 (2018).
40. D. Guo, J. Zhang, B. Zhang, J. Wang, Ruthenium-catalyzed atropoenantioselective synthesis of axial biaryls via reductive amination and dynamic kinetic resolution. *Org. Lett.* **20**, 6284–6288 (2018).
41. D. Guo, Q. Peng, B. Zhang, J. Wang, Atroposelective dynamic kinetic resolution via in situ hemiaminals catalyzed by *N*-heterocyclic carbene. *Org. Lett.* **23**, 7765–7770 (2021).
42. J. A. Carmona, C. Rodríguez-Franco, J. López-Serrano, A. Ros, J. Iglesias-Sigüenza, R. Fernández, J. M. Lassaletta, V. Hornillos, Atroposelective transfer hydrogenation of biaryl aminals via dynamic kinetic resolution. Synthesis of axially chiral diamines. *ACS Catal.* **11**, 4117–4124 (2021).
43. Y. Lv, G. Luo, Q. Liu, Z. Jin, X. Zhang, Y. R. Chi, Catalytic atroposelective synthesis of axially chiral benzonitriles via chirality control during bond dissociation and CN group formation. *Nat. Commun.* **13**, 36 (2022).
44. Z. Zheng, Q. Liu, X. Peng, Z. Jin, J. Wu, NHC-catalyzed chemo- and enantioselective reaction between aldehydes and enals for access to axially chiral arylaldehydes. *Org. Lett.* **26**, 917–921 (2024).

45. X. Hao, Z. Tian, Z. Yao, T. Zang, S. Song, L. Lin, T. Qiao, L. Huang, H. Fu, Atroposelective synthesis of axial biaryls by dynamic kinetic resolution using engineered imine reductases. *Angew. Chem. Int. Ed. Engl.* **63**, e202410112 (2024).
46. S. Staniland, R. W. Adams, J. J. W. McDouall, I. Maffucci, A. Contini, D. M. Grainger, N. J. Turner, J. Clayden, Biocatalytic dynamic kinetic resolution for the synthesis of atropisomeric biaryl *N*-oxide Lewis base catalysts. *Angew. Chem. Int. Ed. Engl.* **55**, 10755–10759 (2016).
47. X. Yuan, J. Wang, Atropoenantioselective synthesis of heterobiaryl *N*-oxides via dynamic kinetic resolution. *Sci. Chin. Chem.* **65**, 2512–2516 (2022).
48. J. A. Carmona, P. Rodríguez-Salamanca, R. Fernández, J. M. Lassaletta, V. Hornillos, Dynamic kinetic resolution of 2-(Quinolin-8-yl) benzaldehydes: Atroposelective iridium-catalyzed transfer hydrogenative allylation. *Angew. Chem. Int. Ed. Engl.* **62**, e202306981 (2023).
49. P. Rodríguez-Salamanca, G. de Gonzalo, J. A. Carmona, J. López-Serrano, J. Iglesias-Sigüenza, R. Fernández, J. M. Lassaletta, V. Hornillos, Biocatalytic atroposelective synthesis of axially chiral *N*-arylindoles via dynamic kinetic resolution. *ACS Catal.* **13**, 659–664 (2023).
50. C. Rodríguez-Franco, A. Ros, P. Merino, R. Fernández, J. M. Lassaletta, V. Hornillos, Dynamic kinetic resolution of indole-based sulfenylated heterobiaryls by rhodium-catalyzed atroposelective reductive aldol reaction. *ACS Catal.* **13**, 12134–12141 (2023).
51. C. Rodríguez-Franco, E. Roldán-Molina, A. Aguirre-Medina, R. Fernández, V. Hornillos, J. M. Lassaletta, Catalytic atroposelective synthesis of C–N axially chiral aminophosphines via dynamic kinetic resolution. *Angew. Chem. Int. Ed. Engl.* **63**, e202409524 (2024).
52. J. M. Coto-Cid, V. Hornillos, R. Fernández, J. M. Lassaletta, G. de Gonzalo, Chemoenzymatic dynamic kinetic resolution of atropoisomeric 2-(Quinolin-8-yl) benzylalcohols. *J. Org. Chem.* **90**, 5120–5124 (2025).

53. N. Kotwal, Tamanna, P. Chauhan, Catalytic asymmetric synthesis of medium-sized bridged biaryls. *Chem. Commun.* **58**, 11031–11044 (2022).
54. X. Yang, L. Wei, Y. Wu, L. Zhou, X. Zhang, Y. R. Chi, Atroposelective access to 1, 3-oxazepine-containing bridged biaryls via carbene-catalyzed desymmetrization of imines. *Angew. Chem. Int. Ed. Engl.* **62**, e202211977 (2023).
55. Z. Wei, Y. Zhao, T. Wang, J. Li, W. Yuan, L. Wei, X. Yang, Bridged biaryl atropisomers by organocatalyzed kinetic asymmetric alcoholysis. *Org. Lett.* **26**, 7110–7115 (2024).
56. X. Bugaut, F. Glorius, Organocatalytic umpolung: *N*-heterocyclic carbenes and beyond. *Chem. Soc. Rev.* **41**, 3511–3522 (2012).
57. S. J. Ryan, L. Candish, D. W. Lupton, Acyl anion free *N*-heterocyclic carbene organocatalysis. *Chem. Soc. Rev.* **42**, 4906–4917 (2013).
58. D. M. Flanigan, F. Romanov-Michailidis, N. A. White, T. Rovis, Organocatalytic reactions enabled by *N*-heterocyclic carbenes. *Chem. Rev.* **115**, 9307–9387 (2015).
59. K. J. R. Murauski, A. A. Jaworski, K. A. Scheidt, A continuing challenge: *N*-heterocyclic carbene-catalyzed syntheses of γ -butyrolactones. *Chem. Soc. Rev.* **47**, 1773–1782 (2018).
60. S. Mondal, S. R. Yetra, S. Mukherjee, A. T. Biju, NHC-catalyzed generation of α,β -unsaturated acylazoliums for the enantioselective synthesis of heterocycles and carbocycles. *Acc. Chem. Res.* **52**, 425–436 (2019).
61. X.-Y. Chen, Z.-H. Gao, S. Ye, Bifunctional *N*-heterocyclic carbenes derived from l-pyroglutamic acid and their applications in enantioselective organocatalysis. *Acc. Chem. Res.* **53**, 690–702 (2020).
62. R. Song, Y. Xie, Z. Jin, Y. R. Chi, Carbene-catalyzed asymmetric construction of atropisomers. *Angew. Chem. Int. Ed. Engl.* **60**, 26026–26037 (2021).
63. K. M. Meragelman, T. C. McKee, M. R. Boyd, 10-Demethoxystegane, A new lignan from *Steganotaenia araliacea*. *J. Nat. Prod.* **64**, 1480–1482 (2001).

64. A. I. Meyers, J. R. Flisak, R. A. Aitken, Asymmetric synthesis of (−)-steganone. Further application of chiral biaryl syntheses. *J. Am. Chem. Soc.* **109**, 5446–5452 (1987).
65. H. Abe, S. Takeda, T. Fujita, K. Nishioka, Y. Takeuchi, T. Harayama, Enantioselective construction of biaryl part in the synthesis of stegane related compounds. *Tetrahedron Lett.* **45**, 2327–2329 (2004).
66. L. G. Monovich, Y. Le Huérou, M. Rönn, G. A. Molander, Total synthesis of (−)-steganone utilizing a samarium(II) iodide promoted 8-endo ketyl–olefin cyclization. *J. Am. Chem. Soc.* **122**, 52–57 (2000).
67. K. Kamikawa, T. Watanabe, A. Daimon, M. Uemura, Stereoselective synthesis of axially chiral natural products, (−)-steganone and O,O'-dimethylkorupensamine A, utilizing planar chiral (Arene)chromium complexes. *Tetrahedron* **56**, 2325–2337 (2000).
68. M. Uemura, A. Daimon, Y. Hayashi, An asymmetric synthesis of an axially chiral biaryl via an (Arene)chromium complex: Formal synthesis of (−)-steganone. *J. Chem. Soc. Chem. Commun.* **1995**, 1943–1944 (1995).
69. B. Yalcouye, S. Choppin, A. Panossian, F. R. Leroux, F. Colobert, A concise atroposelective formal synthesis of (−)-steganone. *Eur. J. Org. Chem.* **2014**, 6285–6294 (2014).
70. Q. Dherbassy, J. Wencel-Delord, F. Colobert, Asymmetric C–H activation as a modern strategy towards expedient synthesis of steganone. *Tetrahedron* **72**, 5238–5245 (2016).
71. S. Takeda, H. Abe, Y. Takeuchi, T. Harayama, Intramolecular biaryl coupling reaction of benzyl benzoate and phenyl benzoate derivatives, and its application to the formal synthesis of (−)-steganone. *Tetrahedron* **63**, 396–408 (2007).
72. S. De Sarkar, S. Grimme, A. Studer, NHC catalyzed oxidations of aldehydes to esters: Chemoselective acylation of alcohols in presence of amines. *J. Am. Chem. Soc.* **132**, 1190–1191 (2010).

73. M. He, J. R. Struble, J. W. Bode, Highly enantioselective azadiene Diels–Alder reactions catalyzed by chiral *N*-heterocyclic carbenes. *J. Am. Chem. Soc.* **128**, 8418–8420 (2006).
74. S. P. Lathrop, T. Rovis, A photoisomerization-coupled asymmetric stetter reaction: Application to the total synthesis of three diastereomers of (−)-cephalimysin A. *Chem. Sci.* **4**, 1668–1673 (2013).
75. M. S. Kerr, T. Rovis, Enantioselective synthesis of quaternary stereocenters via a catalytic asymmetric stetter reaction. *J. Am. Chem. Soc.* **126**, 8876–8877 (2004).
76. P.-C. Chiang, M. Rommel, J. W. Bode, α' -Hydroxyenones as mechanistic probes and scope-expanding surrogates for α,β -unsaturated aldehydes in *N*-heterocyclic carbene-catalyzed reactions. *J. Am. Chem. Soc.* **131**, 8714–8718 (2009).
77. M. Wadamoto, E. M. Phillips, T. E. Reynolds, K. A. Scheidt, Enantioselective synthesis of α,α -disubstituted cyclopentenes by an *N*-heterocyclic carbene-catalyzed desymmetrization of 1,3-diketones. *J. Am. Chem. Soc.* **129**, 10098–10099 (2007).
78. J.-P. Heeb, J. Clayden, M. D. Smith, R. J. Armstrong, R. J., Interrogating the configurational stability of atropisomers. *Nat. Protoc.* **18**, 2745–2771 (2023).
79. O. Trapp, G. Schoetz, V. Schurig, V., Determination of enantiomerization barriers by dynamic and stopped-flow chromatographic methods. *Chirality* **13**, 403–414 (2001).
80. S. Shee, S. Shree Ranganathappa, M. S. Gadhav, R. Gogoi, A. T. Biju, Enantioselective synthesis of C–O axially chiral diaryl ethers by NHC-catalyzed atroposelective desymmetrization. *Angew. Chem. Int. Ed. Engl.* **62**, e202311709 (2023).
81. Y. Wu, X. Guan, H. Zhao, M. Li, T. Liang, J. Sun, G. Zheng, Q. Zhang, Synthesis of axially chiral diaryl ethers via NHC-catalyzed atroposelective esterification. *Chem. Sci.* **15**, 4564–4570 (2024).
82. A. Rosales Martínez, L. Enríquez, M. Jaraíz, L. Pozo Morales, I. Rodríguez-García, E. Díaz Ojeda, A concise route for the synthesis of tetracyclic meroterpenoids: (±)-Aureol preparation and mechanistic interpretation. *Mar. Drugs* **18**, 441 (2020).

83. L. Ding, X. Sui, Z. Gu, Enantioselective synthesis of biaryl atropisomers via Pd/norbornene-catalyzed three-component cross-couplings. *ACS Catal.* **8**, 5630–5635 (2018).
84. S. S. Moleele, J. P. Michael, C. B. de Koning, Tetralones as precursors for the synthesis of 2,2'-disubstituted 1,1'-binaphthyls and related compounds. *Tetrahedron* **64**, 10573–10580 (2008).
85. Y. Zhao, D. G. Truhlar, The M06 suite of density functionals for main group thermochemistry, thermochemical kinetics, noncovalent interactions, excited states, and transition elements: Two new functionals and systematic testing of four M06-class functionals and 12 other functionals. *Theor. Chem. Acc.* **120**, 215–241 (2008).
86. F. Weigend, R. Ahlrichs, Balanced basis sets of split valence, triple zeta valence and quadruple zeta valence quality for H to Rn: Design and assessment of accuracy. *Phys. Chem. Chem. Phys.* **7**, 3297–3305 (2005).
87. F. Weigend, Accurate Coulomb-fitting basis sets for H to Rn. *Phys. Chem. Chem. Phys.* **8**, 1057–1065 (2006).
88. A. V. Marenich, C. J. Cramer, D. G. Truhlar, Universal solvation model based on solute electron density and on a continuum model of the solvent defined by the bulk dielectric constant and atomic surface tensions. *J. Phys. Chem. B* **113**, 6378–6396 (2009).
89. S. Grimme, Supramolecular binding thermodynamics by dispersion-corrected density functional theory. *Chem. A Eur. J.* **18**, 9955–9964 (2012).
90. J. Contreras-García, E. R. Johnson, S. Keinan, R. Chaudret, J.-P. Piquemal, D. N. Beratan, W. Yang, NCIPILOT: A program for plotting noncovalent interaction regions. *J. Chem. Theory Comput.* **7**, 625–632 (2011).